J. Fluid Mech. (1983), vol. 129, pp. 347–364
Printed in Great Britain

Field-flow fractionation

By RONALD SMITH

Department of Applied Mathematics and Theoretical Physics, University of Cambridge, Silver Street, Cambridge CB3 9EW

(Received 1 June 1982 and in revised form 11 October 1982)

If different contaminant species are subject to different transverse drift rates (e.g. gravitational settling), then there is a tendency for the species to separate out. The efficiency of this separation depends upon the relative shapes of the longitudinal concentration distributions. Jayaraj & Subramanian (1978) have drawn attention to the disparity between their computed skew concentration distributions and the symmetric Gaussian distributions predicted by one-dimensional diffusion models. Here it is shown that a one-dimensional delay-diffusion model yields suitably skew predictions. The model equation is used to investigate the extent to which the separation of different contaminant species can be improved by pre-treating the sample (i.e. allowing differential drift) in a stationary fluid before being eluted into the shear flow. Pretreatment is found to be very effective for plane Poiseuille flow but not for the thermogravitational columns.

1. Introduction

In a laminar or turbulent shear flow the advection velocity for a cloud of contaminant depends upon the concentration profile across the flow. If different contaminant species have different equilibrium profiles, then they will eventually travel at different velocities. Field-flow fractionation is a class of processes which exploit this effect to separate the constituents of a mixture (Kirkwood & Brown 1952; Taggart 1953; Lightfoot, Chiang & Noble 1981). A force field (electrical, magnetic, thermal, centrifugal or gravitational) is used to induce a species-dependent drift velocity across the flow, and thereby controls the equilibrium profiles.

The efficiency of the separation can be severely reduced by the longitudinal spreading of the individual constituents. Giddings (1968) showed that at sufficiently large times after discharge the longitudinal dispersion process can be described by a one-dimensional constant-coefficient diffusion equation. Thus the linear rate of separation eventually dominates the square-root rate of spreading.

In practice the time needed for the diffusion equation to become applicable can be prohibitively large. Also, for extraction processes it is desirable to avoid excessive dilution, and therefore deliberately to restrict the amount of time available for longitudinal spreading. This led Krishnamurthy & Subramanian (1977) to investigate the transient stages by means of a one-dimensional variable-coefficient diffusion equation, with the longitudinal-dispersion coefficient changing with time.

For a point discharge the longitudinal concentration distribution predicted by the variable-coefficient diffusion equation is Gaussian and exactly symmetric. Alas, Jayaraj & Subramanian (1978) showed computationally that, for the particular case of laminar flow in a parallel-plate channel, the longitudinal concentration distributions are markedly skew, with concentration peaks significantly displaced from the Gaussian predictions. Depending upon the relative shifts of the concentration peaks, this can have a major influence upon the efficiency of separation.

Recently, the author (Smith 1981) has shown that for laminar or turbulent flows when there is no transverse drift the skewness of the longitudinal concentration distribution can be reproduced exactly by a one-dimensional delay-diffusion equation. The purpose of the present paper is to show how transverse drift can be allowed for in the delay-diffusion model. As we might hope, the new predicted longitudinal concentration distributions are in good agreement with the results of Jayaraj & Subramanian (1978).

It is the perturbation of the concentration profile from equilibrium which gives rise to the shear dispersion (Giddings 1968). In the one-dimensional diffusion approach, this perturbation is related to the local longitudinal concentration gradient (Krishnamurthy & Subramanian 1977). The actual response of the cross-stream concentration profile is not instantaneous. The delay-diffusion approach allows for the fading influence of the longitudinal concentration gradient further upstream at earlier times. The skewness is towards the front or rear according to whether the memory velocity is faster or slower than the centroid velocity (Smith 1981).

One advantage of using a model equation, rather than the full equations, is that it is comparatively easy to investigate a range of conditions. In particular, §8 of this paper tests the effectiveness of pretreating a sample by application of the transverse field in a stationary fluid prior to elution. The idea is that the concentration profile for each constituent is already equilibrated, thereby maximizing the initial velocity difference. For plane Poiseuille flow this technique is found to provide significantly improved separation of the different constituents. However, for a free-convection flow (thermogravitational column), there is only a slight improvement in separation.

2. Longitudinal-dispersion equation

If there is a drift velocity v across the primary flow $u(y)$, then the advection–diffusion equation for the contaminant concentration $c(x, y, t)$ takes the form

$$\partial_t c + u\,\partial_x c + \partial_y(vc) - \kappa\,\partial_x^2 c - \partial_y(\kappa\,\partial_y c) = q, \tag{2.1a}$$

with

$$vc - \kappa\,\partial_y c = 0 \quad (y = y_-, y_+). \tag{2.1b}$$

Here $\kappa(y)$ is the diffusivity, $q(x, y, t)$ the source strength, and y_-, y_+ the positions of the impermeable boundaries. In a turbulent fluid it is necessary that the contaminant be very dilute (so that the drift of contaminant does not modify the turbulence), and that v be small (so that a contaminant particle stays within an eddy long enough that the effects of the turbulence can be modelled by means of the eddy diffusivity).

The equilibrium profile of concentration across the flow is given by

$$\gamma(y) = \exp\left(\int_{y_0}^{y} \frac{v}{\kappa}\,\mathrm{d}y'\right), \quad \bar{\gamma} = 1, \tag{2.2a,b}$$

where the reference level y_0 is chosen so that the cross-sectional average value $\bar{\gamma} = 1$ is correctly reproduced. To study the way in which the concentration approaches this equilibrium profile, we make the decomposition

$$c = \bar{c}(x, t)\,\gamma(y) + c', \quad q = \bar{q}(x, t)\,\gamma(y) + q', \tag{2.3a,b}$$

where the correction terms c', q' have zero cross-sectional average values.

For mathematical simplicity we shall first analyse the pretreated case in which the

initial discharge exactly conforms to the equilibrium profile (i.e. $q' = 0$). Following Smith (1981, equation (1.5)) we pose the series representation

$$c' = \sum_{j=1}^{\infty} \int_0^{\infty} l_j(y,\tau)\, \partial_x^j \bar{c}\left(x - \int_0^{\tau} \tilde{u}(\tau')\,\mathrm{d}\tau', t-\tau\right)\mathrm{d}\tau. \tag{2.4}$$

Thus the concentration variations across the flow induced by the velocity shear depend upon the upstream conditions at previous times, with weight functions $l_j(y,\tau)$ and displacement velocity $\tilde{u}(\tau)$. Substituting this representation into equation (2.1*a*) and then taking the cross-sectional average value, we obtain an exact evolution equation for $\bar{c}$:

$$\partial_t \bar{c} + \overline{\gamma u}\,\partial_x \bar{c} - \overline{\kappa\gamma}\,\partial_x^2 \bar{c} + \sum_{j=1}^{\infty} \int_0^{\infty} \overline{l_j u}\,\partial_x^{j+1} \bar{c}\left(x - \int_0^{\tau} \tilde{u}(\tau')\,\mathrm{d}\tau', t-\tau\right)\mathrm{d}\tau$$
$$- \sum_{j=1}^{\infty} \int_0^{\infty} \overline{\kappa l_j}\,\partial_x^{j+2} \bar{c}\left(x - \int_0^{\tau} \tilde{u}(\tau')\,\mathrm{d}\tau', t-\tau\right)\mathrm{d}\tau = \bar{q}. \tag{2.5}$$

Neglecting $\partial_x^3 \bar{c}$ and higher derivatives yields the delay-diffusion equation

$$\partial_t \bar{c} + u_{00}\,\partial_x \bar{c} - \kappa_{00}\,\partial_x^2 \bar{c} - \int_0^{\infty} \partial_\tau D\,\partial_x^2 \bar{c}\left(x - \int_0^{\tau} \tilde{u}(\tau')\,\mathrm{d}\tau', t-\tau\right)\mathrm{d}\tau = \bar{q}, \tag{2.6}$$

with

$$u_{00} = \overline{\gamma u}, \quad \kappa_{00} = \overline{\kappa\gamma}, \quad \partial_\tau D = -\overline{u l_1}. \tag{2.7a,b,c}$$

Lure & Maron (1979) derived a similar delay-diffusion equation, but with an additional $\partial_x \bar{c}$ memory integral and without the displacement velocity $\tilde{u}(\tau)$ (i.e. a more complicated equation which does not reproduce the exact skewness).

3. Memory functions

The formally exact equation (2.5) permits us to replace time derivatives in favour of x-derivatives. Thus, as shown in detail by Smith (1981, equation (2.4)), we can extract from the field equation (2.1*a*) the equations satisfied by the weight functions $l_j(y,\tau)$ (i.e. the coefficients of $\partial_x^j \bar{c}$):

$$\partial_\tau l_1 + \partial_y(v l_1) - \partial_y(\kappa\,\partial_y l_1) = 0, \tag{3.1a}$$

with

$$v l_1 - \kappa\,\partial_y l_1 = 0 \quad (y = y_-, y_+), \tag{3.1b}$$

$$l_1 = (\overline{u\gamma} - u)\gamma \quad (\tau = 0), \tag{3.1c}$$

$$\partial_\tau l_2 + \partial_y(v l_2) - \partial_y(\kappa\,\partial_y l_2) = \tilde{u} l_1 + \gamma\overline{u l_1} - u l_1, \tag{3.2a}$$

with

$$v l_2 - \kappa\,\partial_y l_2 = 0 \quad (y = y_-, y_+), \tag{3.2b}$$

$$l_2 = (\kappa - \overline{\kappa\gamma})\gamma \quad (\tau = 0). \tag{3.2c}$$

The drift term in (3.1*a*) can be removed by means of the change of variables

$$l_1(y,\tau) = \gamma^{\frac{1}{2}} L(y,\tau). \tag{3.3}$$

The resulting equations for L can be written

$$\partial_\tau L + \left[\tfrac{1}{2}\partial_y v + \frac{v^2}{4\kappa}\right] L - \partial_y(\kappa\,\partial_y L) = 0, \tag{3.4a}$$

with
$$\tfrac{1}{2}vL-\kappa\,\partial_y L=0 \quad (y=y_-,y_+), \tag{3.4b}$$
$$L=(\overline{u\gamma}-u)\,\gamma^{\frac{1}{2}} \quad (\tau=0). \tag{3.4c}$$

To solve (3.4*a–c*) we introduce the eigenfunctions $\psi_m(y)$:
$$\frac{\mathrm{d}}{\mathrm{d}y}\left(\kappa\frac{\mathrm{d}\psi_m}{\mathrm{d}y}\right)+\left[\lambda_m-\tfrac{1}{2}\partial_y v-\frac{v^2}{4\kappa}\right]\psi_m=0, \tag{3.5a}$$
with
$$\tfrac{1}{2}v\psi_m-\kappa\,\partial_y\psi_m=0 \quad (y=y_-,y_+), \tag{3.5b}$$
$$\psi_0=\gamma^{\frac{1}{2}}, \quad \overline{\psi_m\psi_n}=\delta_{mn}, \tag{3.5c,d}$$
where δ_{mn} is the Kronecker delta. For the initial conditions (3.4*c*) at $\tau=0$, we are led to define the velocity coefficients
$$u_{mn}=\overline{u\psi_m\psi_n}, \quad \gamma^{\frac{1}{2}}u(y)=\sum_{m=0}^{\infty}u_{m0}\,\psi_m(y). \tag{3.6a,b}$$
Thus the solution of (3.4*a–c*) is given by the series
$$L=-\sum_{m=1}^{\infty}u_{m0}\,\psi_m(y)\exp(-\lambda_m\tau). \tag{3.7}$$

We recall that the memory function $\partial_\tau D$ in the delay-diffusion equation (2.6) is given by
$$\partial_\tau D=-\overline{ul_1}=-\overline{\gamma^{\frac{1}{2}}uL}. \tag{3.8}$$
Substituting for $\gamma^{\frac{1}{2}}u$ and L in terms of their respective eigenfunction expansions (3.6*b*, 3.7), we arrive at the neat expression
$$\partial_\tau D=\sum_{m=1}^{\infty}u_{m0}^2\exp(-\lambda_m\tau). \tag{3.9}$$
This shows that the memory function is strictly positive and decays exponentially on a timescale of $1/\lambda_1$.

4. Memory displacement velocity

Formally (3.9) is identical with the corresponding result of Smith (1981, equation (3.4)). Indeed, what has been achieved through the introduction of the eigenmodes (3.5) is the elimination of any explicit occurrence of the transverse drift velocity. Thus, we can straightforwardly adapt any of the results of Smith (1981). In particular, the truncated equation (2.6) is at its most accurate if the coefficient $(\overline{ul_2}-\overline{\kappa l_1})$ of $\partial_x^3\bar{c}$ in (2.5) is zero. Field-flow fractionation is viable only when advection effects dominate diffusion, i.e. when the diffusivity κ is relatively small. In this high-Péclet-number limit, or when κ is constant, the vanishing of the $\partial_x^3\bar{c}$ coefficient is achieved if we select the memory velocity $\tilde{u}(\tau)$:
$$\partial_\tau D\int_0^\tau[\tilde{u}(\tau')-u_{00}]\,\mathrm{d}\tau'=\tau\sum_{m=1}^{\infty}(u_{mm}-u_{00})\,u_{m0}^2\exp(-\lambda_m\tau)$$
$$+\sum_{m=1}^{\infty}\sum_{n\neq m}u_{mn}\,u_{m0}\,u_{n0}\left\{\frac{\exp(-\lambda_n\tau)-\exp(-\lambda_m\tau)}{\lambda_m-\lambda_n}\right\} \tag{4.1}$$
(Smith 1981, equation (4.6)).

As noted by Smith (1981, §4), if (2.5) is multiplied by x^n and integrated from $-\infty$ to $+\infty$, then only terms up to $\partial_x^n\bar{c}$ contribute to the evolution of the nth moment

$\bar{c}^{(n)}$. Thus, if the coefficient of $\partial_x^3 \bar{c}$ is negligible, then the truncated equation (2.6) yields exact results for $\bar{c}^{(3)}$ as well as for the lower moments $\bar{c}^{(0)}$, $\bar{c}^{(1)}$, $\bar{c}^{(2)}$. Hence with the optimum selection (4.1) for the memory displacement velocity, the area, centroid, variance and skewness are all exactly reproduced by the delay-diffusion equation (2.6).

The connection between the displacement velocity and the skewness can be seen in the formula

$$\partial_t \bar{c}^{(3)} = 6\bar{c}^{(0)} \int_0^t \partial_\tau D \int_0^\tau [\tilde{u}(\tau') - u_{00}] \, \mathrm{d}\tau' \, \mathrm{d}\tau \tag{4.2}$$

(Smith 1981, equation (4.9)). Thus, when the memory velocity $\tilde{u}$ exceeds the centroid velocity u_{00}, there is a tendency to develop positive skewness (i.e. a forwards tail). The weight factor $\partial_\tau D$ gives greatest importance to the value of $\tilde{u} - u_{00}$ at times less than the memory scale $1/\lambda_1$.

The physical origin of the skewness lies in the velocity profile across the flow (see the pure convection solution in figure 3 of Jayaraj & Subramanian 1978). In particular, from (4.1) and the definitions (3.6*a*, *b*), we can derive the result

$$\tilde{u}(0) - u_{00} = \frac{\overline{\gamma(u-u_{00})^3}}{\overline{\gamma(u-u_{00})^2}}. \tag{4.3}$$

The cubic emphasizes extremes of the difference between the local and the weighted-mean velocities. Thus large u_{00} can be associated with negative skewness, and small u_{00} with positive skewness (contrast figures 4 and 14 of Jayaraj & Subramanian 1978).

5. General discharges

For simplicity the above derivation of the delay-diffusion equation (2.6) was based on the assumption that the source distribution $q(x, y, t)$ conformed exactly to the equilibrium profile $\gamma(y)$ across the flow. The most usual situation, of a uniform discharge, does not satisfy this assumption. Follwing Smith (1982), the necessary generalization is to represent $q(x, y, t)$ as

$$q = \bar{q}(x, t)\, \gamma(y) + \gamma^{\frac{1}{2}} \sum_{m=1}^{\infty} q_m(x, t)\, \psi_m(y), \tag{5.1}$$

and to include additional source-memory terms in the series (2.4):

$$\sum_{m=1}^{\infty} \sum_{j=0}^{\infty} \int_0^\infty f_{mj}(y, \tau)\, \partial_x^j q_m \left(x - \int_0^\tau \tilde{u}_m(\tau') \, \mathrm{d}\tau', t - \tau \right) \mathrm{d}\tau. \tag{5.2}$$

This leads to further right-hand-side terms in the exact evolution equation (2.5) for $\bar{c}$:

$$\sum_{m=1}^{\infty} \sum_{j=1}^{\infty} \int_0^\infty [\overline{\kappa f_{m\,j-2}} - \overline{u f_{m\,j-1}}]\, \partial_x^j q_m \left(x - \int_0^\tau \tilde{u}_m(\tau') \, \mathrm{d}\tau', t - \tau \right) \mathrm{d}\tau. \tag{5.3}$$

A minimal description of the effects of the cross-stream discharge profile is to retain just the $\partial_x q_m$ terms. When this is optimized by the section of $\tilde{u}_m$ (i.e. the absence of a $\partial_x^2 q_m$ term), we arrive at the delay-diffusion equation

$$\partial_t \bar{c} + u_{00}\, \partial_x \bar{c} - \kappa_{00}\, \partial_x^2 \bar{c} - \int_0^\infty \partial_\tau D\, \partial_x^2 \bar{c} \left(x - \int_0^\tau \tilde{u}(\tau') \, \mathrm{d}\tau', t - \tau \right) \mathrm{d}\tau$$

$$= \bar{q} - \sum_{m=1}^{\infty} \int_0^\infty \exp(-\lambda_m \tau)\, \partial_x q_m(x - u_{mm}\tau, t - \tau) \, \mathrm{d}\tau \tag{5.4}$$

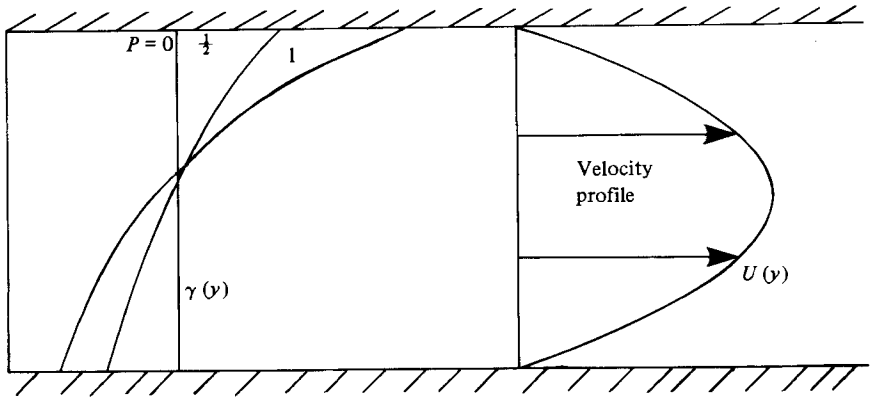

FIGURE 1. The velocity and equilibrium concentration profiles for plane Poiseuille flow.

(Smith 1982, equation (5.2)). The optimization ensures that (5.4) gives the exact area, centroid and variance for arbitrary discharge profiles.

The variable coefficient diffusion equation

$$\partial_t \bar{c} - K_1(t)\,\partial_x \bar{c} - K_2(t)\,\partial_x^2 \bar{c} = 0 \tag{5.5}$$

derived by Krishnamurthy & Subramarian (1978) also has the virtue of yielding exact results for the area, centroid and variance. In the present notation the K_1, K_2 coefficients for a sudden discharge at $t = 0$ are

$$K_1(t) = -u_{00} - \sum_{m=1}^{\infty} q_m u_{m0} \exp(-\lambda_m t), \tag{5.6}$$

$$K_2(t) = \kappa_{00} + D(t) + \sum_{m=1}^{\infty} q_m u_{m0}(u_{mm} - u_{00})\, t \exp(-\lambda_m t) - \left[\sum_{m=1}^{\infty} \frac{q_m u_{m0}}{\lambda_m}\{1 - \exp(-\lambda_m \tau)\}\right]\left[\sum_{m=1}^{\infty} q_m u_{m0} \exp(-\lambda_m \tau)\right]. \tag{5.7}$$

Thus, unless the q_m terms are absent, the coefficients are more difficult to calculate than the corresponding coefficients in the delay-diffusion equation (4.4). A more serious shortcoming of the diffusion model is that it is inapplicable to repeated or multiple (non-identical) discharges (Smith 1981, 1982).

6. Plane Poiseuille flow

For steady laminar flow between parallel plates a distance h apart, the horizontal velocity profile is parabolic:

$$u(y) = 6\bar{u}\left[\frac{y}{h} - \left(\frac{y}{h}\right)^2\right] \quad (0 \leqslant y \leqslant h). \tag{6.1}$$

If the transverse drift velocity v and the diffusivity κ are both constant, then the equilibrium profile of concentration across the flow is exponential (see figure 1)

$$\gamma = \frac{2P \exp(2P(y/h))}{\exp(2P) - 1}, \tag{6.2}$$

where

$$P = vh/2\kappa. \tag{6.3}$$

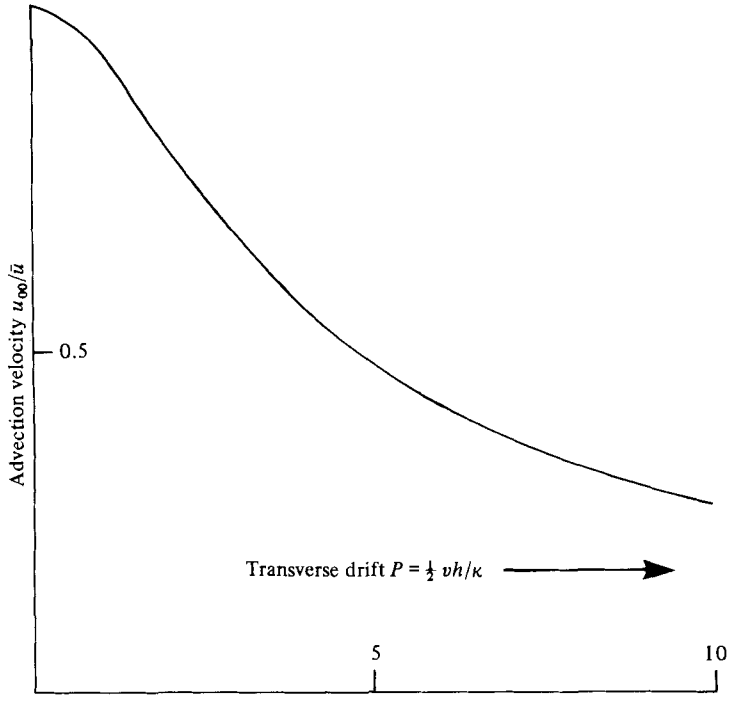

FIGURE 2. The asymptotic longitudinal centroid velocity u_{00} as a function of the transverse drift velocity for plane Poiseuille flow.

The weighted average advection velocity u_{00} is given by

$$u_{00} = \frac{3\bar{u}[P \coth P - 1]}{P^2} \tag{6.4}$$

(Krishnamurthy & Subramanian 1977, equation (A 18)). For small transverse drift the reduction in concentration near one boundary is compensated by an increase in concentration at the other boundary. Thus, the reduction in the advection velocity is quadratic in P. In the opposite limit of large transverse drift, the equilibrium concentration profile (6.2) only penetrates a distance of order h/P away from the boundary. This leads to the advection velocity decreasing as $\bar{u}/P$ (see figure 2 and Krishnamurthy & Subramanian 1977, figure 3). We remark that to achieve efficient separation of different species it would be desirable to adjust the force field so that the transverse Péclet numbers P_j for the constituents lie in the range 2–10.

The eigenfunctions $\psi_m(y)$ are displaced sinusoids:

$$\begin{aligned}\psi_m &= \sqrt{2}\cos\left[\frac{m\pi y}{h} - \arctan^{-1}\frac{P}{m\pi}\right] \\ &= \sqrt{2}\left\{m\pi\cos\frac{m\pi y}{h} + P\sin\frac{m\pi y}{h}\right\}[m^2\pi^2 + P^2]^{-\frac{1}{2}},\end{aligned} \tag{6.5}$$

with

$$\lambda_m = [m^2\pi^2 + P^2]\frac{\kappa}{h^2}. \tag{6.6}$$

The dependence of the decay rates upon the drift velocity v (i.e. upon P) shows that

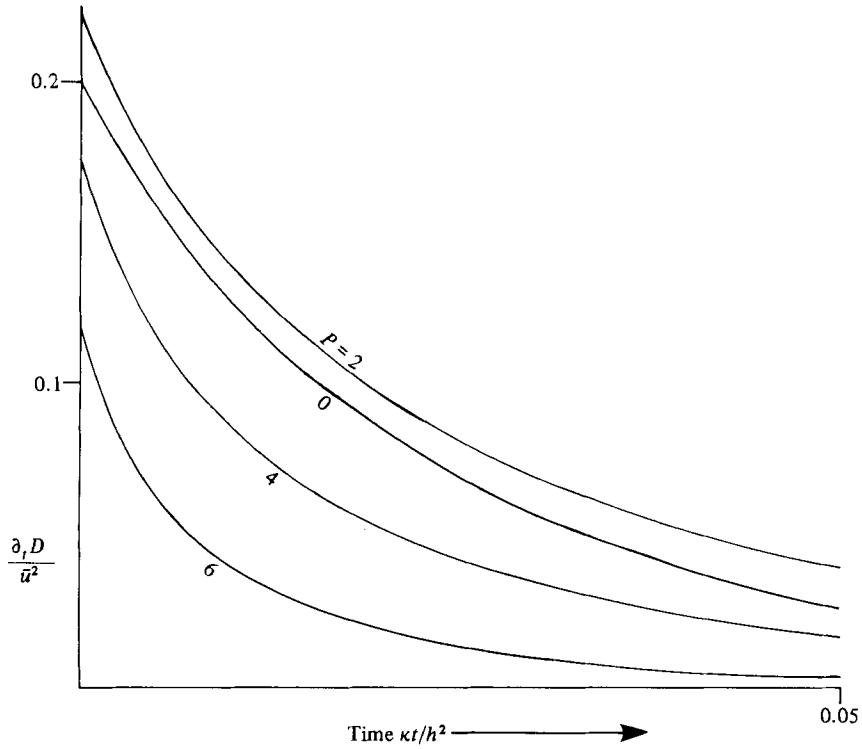

FIGURE 3. The decay of the memory function $\partial_\tau D$ for different values of the transverse Péclet number in plane Poiseuille flow.

the transverse bodily moment of the entire contaminant profile accelerates the free (x-independent) decay towards the equilibrium profile.

Multiplying together u, $\gamma^{\frac{1}{2}}$, ψ_m and then taking the cross-sectional average value, we arrive at the result

$$u_{m0} = -\bar{u}\,12\sqrt{2}\left\{\frac{P}{\sinh P}\right\}^{\frac{1}{2}} \frac{m\pi}{[m^2\pi^2+P^2]^{\frac{3}{2}}}\left\{\cosh\tfrac{1}{2}P - \frac{4P\sinh\frac{1}{2}P}{m^2\pi^2+P^2}\right\} \quad (m \text{ even}), \tag{6.7a}$$

$$u_{m0} = \bar{u}\,12\sqrt{2}\left\{\frac{P}{\sinh P}\right\}^{\frac{1}{2}} \frac{m\pi}{[m^2\pi^2+P^2]^{\frac{3}{2}}}\left\{\sinh\tfrac{1}{2}P - \frac{4P\cosh\frac{1}{2}P}{m^2\pi^2+P^2}\right\} \quad (m \text{ odd}) \tag{6.7b}$$

(Gradshteyn & Ryzhik 1980, §2.667). The general expression (3.9) now permits us to evaluate the delay-diffusion function $\partial_\tau D$ (see figure 3). For $P = 0$ only the even coefficients are non-zero. Thus for small values of the transverse drift, the symmetry breaking leads to an increased and greatly prolonged memory, primarily associated with the leading odd coefficient u_{10}. The centre of the flow and the boundary are regions in which the shear-dispersion process is least efficient. For small P there is less material near the centre (see figure 1), so the delay-dispersion function is increased. However, for large P the contaminant becomes so tightly confined to the boundary that $\partial_\tau D$ is reduced.

The higher-order velocity coefficients u_{mn} are given by

$$u_{mm} = \bar{u}\left(1 - \frac{3(m^2\pi^2-P^2)}{m^2\pi^2(m^2\pi^2+P^2)}\right), \tag{6.8a}$$

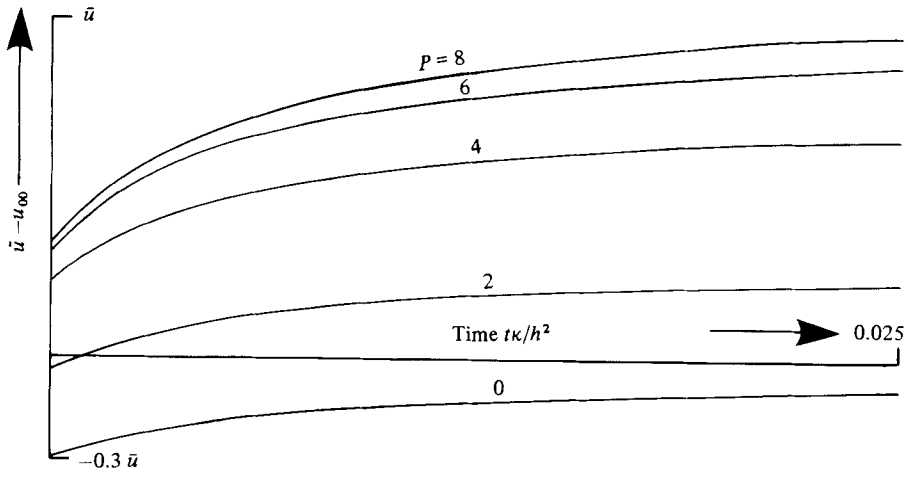

FIGURE 4. The memory displacement velocity $\tilde{u}(\tau) - u_{00}$ for plane Poiseuille flow, showing the change from small negative to large positive displacements (skewness) when the transverse drift parameter P is increased.

$$u_{mn} = \frac{-96\bar{u}mnP}{\pi^2(m^2-n^2)^2\,[m^2\pi^2+P^2]^{\frac{1}{2}}\,[n^2\pi^2+P^2]^{\frac{1}{2}}} \quad (m+n \text{ odd}), \tag{6.8b}$$

$$u_{mn} = \frac{-24\bar{u}mn(m^2\pi^2+n^2\pi^2+2P^2)}{\pi^2(m^2-n^2)^2\,[m^2\pi^2+P^2]^{\frac{1}{2}}\,[n^2\pi^2+P^2]^{\frac{1}{2}}} \quad (m+n \text{ even}). \tag{6.8c}$$

Figure 4 shows the time dependence of the memory displacement velocity $\tilde{u}(\tau) - u_{00}$ which results from using these expressions for u_{mn} in (4.1). For weak transverse drift there is a reduction in the magnitude of the velocity difference $\tilde{u} - u_{00}$. However, for larger P, the velocity difference becomes quite marked, but of reversed sign.

The implied changeover from negative to positive skewness is in qualitative agreement with the numerical results of Jayaraj & Subramanian (1978, figures 4, 13). Positive skewness implies that the concentration peak will be displaced to the left of the centroid. Thus, for a mixture of two contaminants, not only will the contaminant with the larger value of P have a slower centroid velocity u_{00}, but also there will be an additional displacement to the left for the concentration peak. Hence the true separation of constituents in plane Poiseuille flow is more efficient than would be predicted in a diffusion approximation (Krishnamurthy & Subramanian 1977).

For a uniform discharge $q(x,t)$, the eigencoefficients q_m are given by

$$\frac{q_m}{\bar{q}} = 2\sqrt{2}\left\{\frac{\sinh P}{P}\right\}^{\frac{1}{2}} \sinh \tfrac{1}{2}P \quad (m \text{ even}), \tag{6.9a}$$

$$\frac{q_m}{\bar{q}} = 2\sqrt{2}\left\{\frac{\sinh P}{P}\right\}^{\frac{1}{2}} \cosh \tfrac{1}{2}P \quad (m \text{ odd}). \tag{6.9b}$$

Figure 5 shows how the centroid velocity

$$u_{00} + \sum_{m=1}^{\infty} \frac{q_m}{\bar{q}} u_{m0} \exp(-\lambda_m t) \tag{6.10}$$

decreases to u_{00} as the contaminant profile across the flow relaxes towards its asymptotic state (Krishnamurthy & Subramanian 1977, equation (A 17) and figure

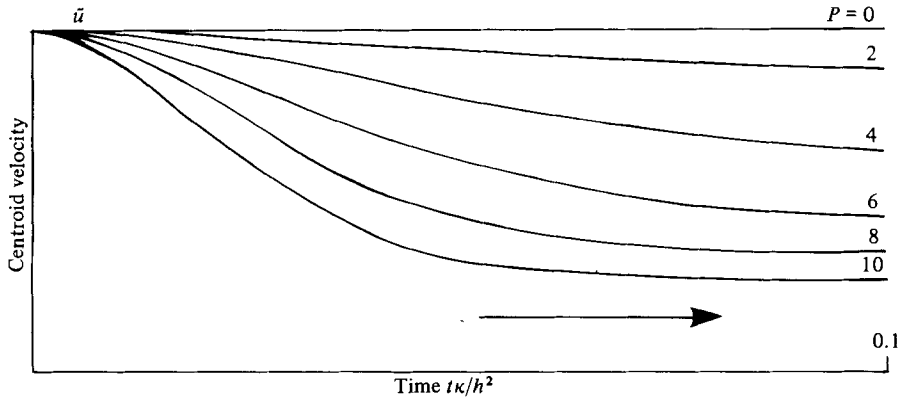

FIGURE 5. The centroid velocity as a function of time for an initially uniform discharge in plane Poiseuille flow.

2). A noteworthy feature is that near $t = 0$ the centroid velocity only departs very gradually from the bulk velocity $\bar{u}$. The reason for this is the symmetry of the velocity profile. For small times the reduced concentration in one half of the flow is counterbalanced by the increased concentration in the other half of the flow.

For a mixture of two constituents with transverse Péclet numbers P_1, P_2 the separation of the centroids is proportional to the area between the respective curves in figure 5. Thus the separation is dismayingly inefficient until times of order $0.05h^2/\kappa$. Jayaraj & Subramanian (1978, figures 3, 12) give the concentration distributions for $P = 0, 5$ at the very early time $0.025h^2/\kappa$. In keeping with the above discussion, the separation is barely perceptible. It deserves comment that at such early times the shear-dispersion process is decidedly two-dimensional (Jayaraj & Subramanian 1978, figures 2 and 7), and the concentration profiles across the flow are too far away from the equilibrium for the one-dimensional diffusion or delay-diffusion models to be meaningful (Smith 1982, figure 2).

Although the above figures 1–5 do illuminate the effects of transverse drift upon contaminant dispersion, they do not provide a test of the accuracy of the delay-diffusion equation. To do this, (5.4) was solved numerically for the particular case

$$P = 5, \quad t = 0.5\frac{h^2}{\kappa}, \quad \frac{\kappa}{h\bar{u}} = 0.001, \quad q = 100 \quad \text{for} \quad \left|\frac{x\kappa}{\bar{u}h^2}\right| < 0.005. \tag{6.11}$$

Figures 9, 10 of Jayaraj & Subramanian (1978) show that at this relatively large time the transverse concentration profile is close to equilibrium. Thus reasonable results can be expected of a one-dimensional model. Figure 6 confirms that this is indeed the case. Reassuringly, the delay-diffusion equation is much more accurate than the diffusion equation, with the concentration peak significantly reduced and shifted to the left.

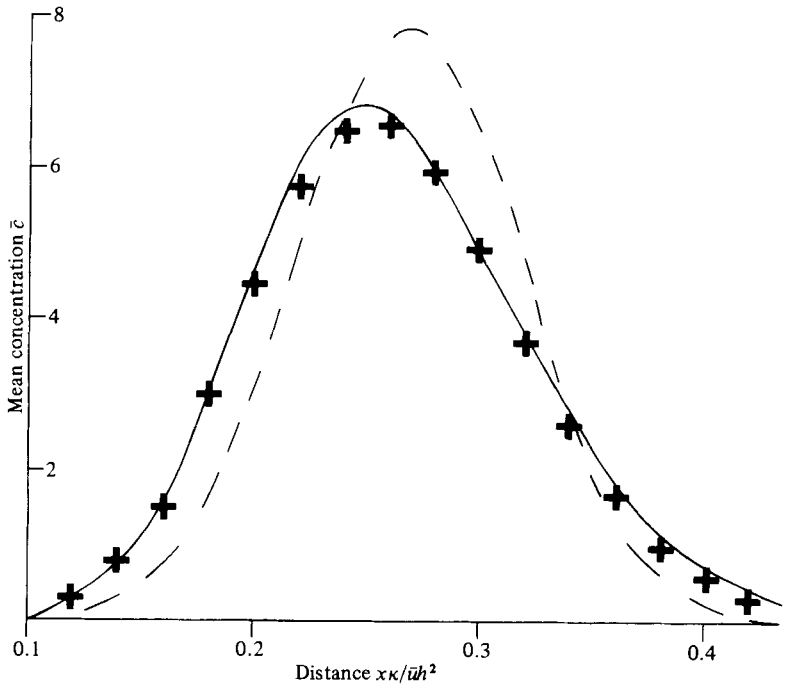

FIGURE 6. Exact (——), delay-diffusion (+ + +) and diffusion (— — —) concentration profiles for plane Poiseuille flow with transverse drift.

7. Thermogravitational columns

A temperature difference between the two walls of a vertical channel gives rise to the velocity field

$$u = 16U\left[-\frac{y}{h}+3\left(\frac{y}{h}\right)^2-2\left(\frac{y}{h}\right)^3\right] \quad (0 \leqslant y \leqslant h) \tag{7.1}$$

(see figure 7 and Lightfoot *et al.* 1981, figure 3*c*), where U is the mean velocity in the upwards-going half of the flow. Conveniently, the equilibrium concentration profile $\gamma(y)$ and the eigenfunctions $\psi_m(y)$ are precisely the same as for plane Poiseuille flow ((6.2), (6.5)).

The weighted average advection velocity is given by

$$u_{00} = 8U\{P^2+3-3P\coth P\}/P^3, \tag{7.2}$$

with

$$P = vh/2\kappa \tag{7.3}$$

(see figure 8). The up–down symmetry of the flow permits us to restrict our attention to positive values of the transverse Péclet number P. For small P there is more contaminant in the upwards-going half of the flow, and there is a marked increase in u_{00}. However, for large transverse drift the contaminant is so closely confined to the wall that u_{00} eventually decreases as U/P. The maximum advection velocity (of $0.88U$) is attained at $P = 3.5$. Thus, for efficient separation of different constituents it is desirable to keep the transverse force field sufficiently weak that the transverse Péclet numbers P_j are all in the range -3.5 to $+3.5$ (i.e. to avoid the possibility of two contaminant species with different P_j having the same equilibrium velocity u_{00}).

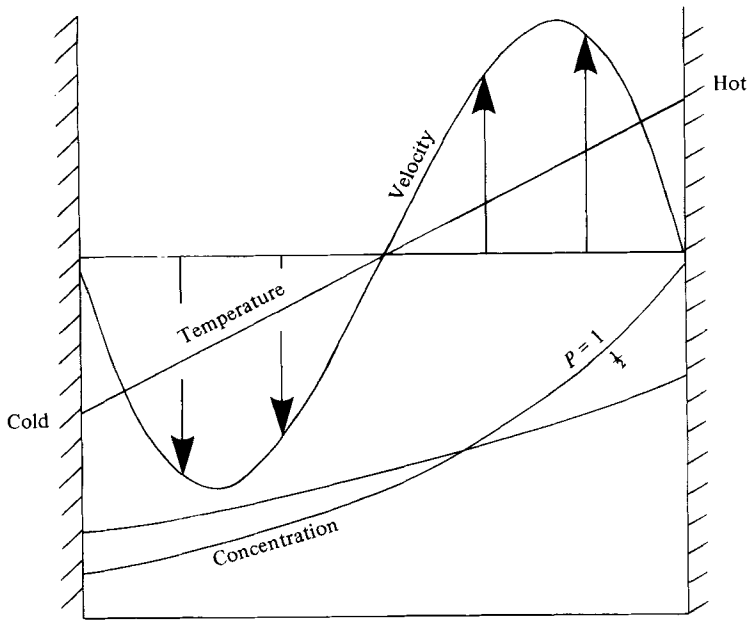

FIGURE 7. The velocity and equilibrium concentration profiles for a thermogravitational column.

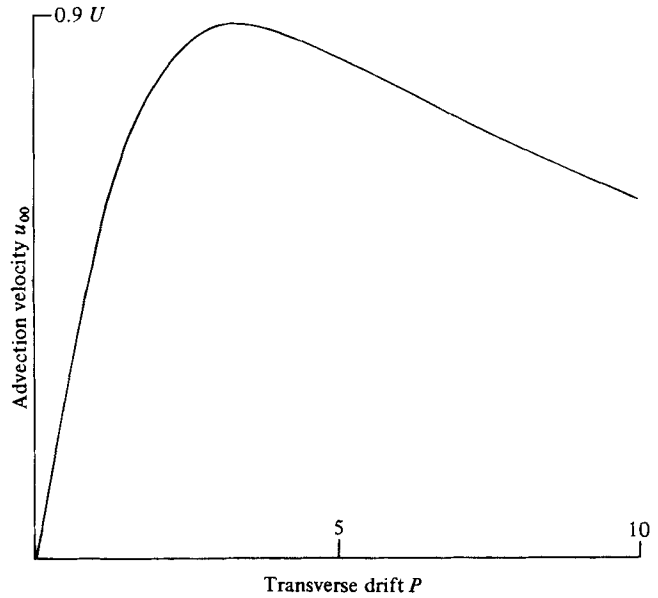

FIGURE 8. The asymptotic centroid velocity u_{00} as a function of the transverse drift velocity for a thermogravitational column.

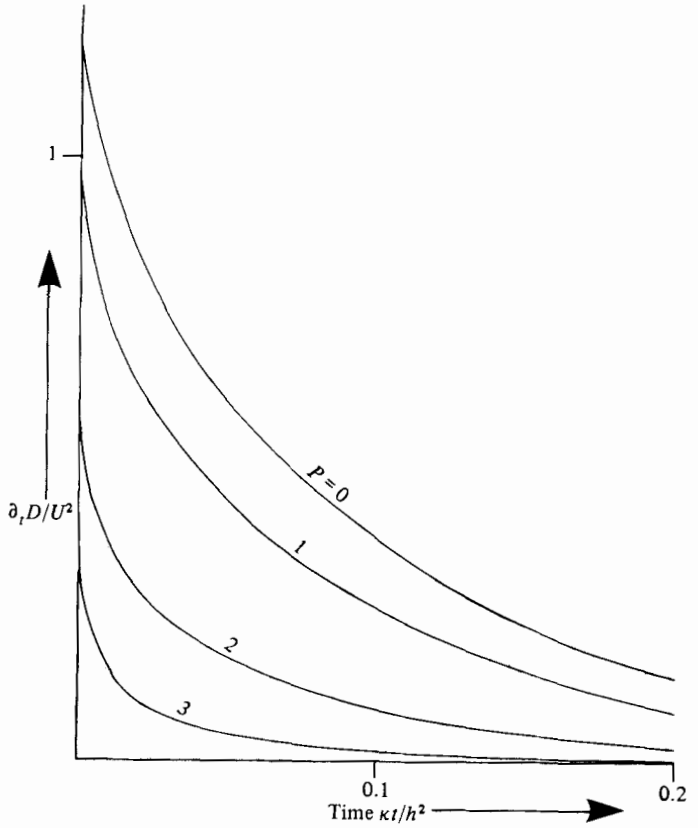

FIGURE 9. The decay of the memory function $\partial_\tau D$ for different values of the transverse Péclet number in a thermogravitational column.

Performing the integral $\overline{u\gamma^{\frac{1}{2}}\psi_m}$ (Gradshteyn & Ryzhik 1980, §2.667), we obtain the coefficients

$$u_{m0} = -U32\sqrt{2}\left\{\frac{P}{\sinh P}\right\}^{\frac{1}{2}}\frac{m\pi}{[m^2\pi^2+P^2]^{\frac{3}{2}}}\left\{\left[1+\frac{12(3P^2-m^2\pi^2)}{[m^2\pi^2+P^2]^2}\right]\sinh\tfrac{1}{2}P - \frac{12P}{m^2\pi^2+P^2}\cosh\tfrac{1}{2}P\right\} \quad (m \text{ even}), \tag{7.4a}$$

$$u_{m0} = U32\sqrt{2}\left\{\frac{P}{\sinh P}\right\}^{\frac{1}{2}}\frac{m\pi}{[m^2\pi^2+P^2]^{\frac{3}{2}}}\left\{\left[1+\frac{12(3P^2-m^2\pi^2)}{[m^2\pi^2+P^2]^2}\right]\cosh\tfrac{1}{2}P - \frac{12P}{m^2\pi^2+P^2}\sinh\tfrac{1}{2}P\right\} \quad (m \text{ odd}). \tag{7.4b}$$

Figure 9 shows the delay-dispersion function $\partial_\tau D$ which results from using these coefficients in the summation (3.9). The much greater shear in the free-convection velocity profile (figure 7) as compared with plane Poiseuille flow (figure 1) gives rise

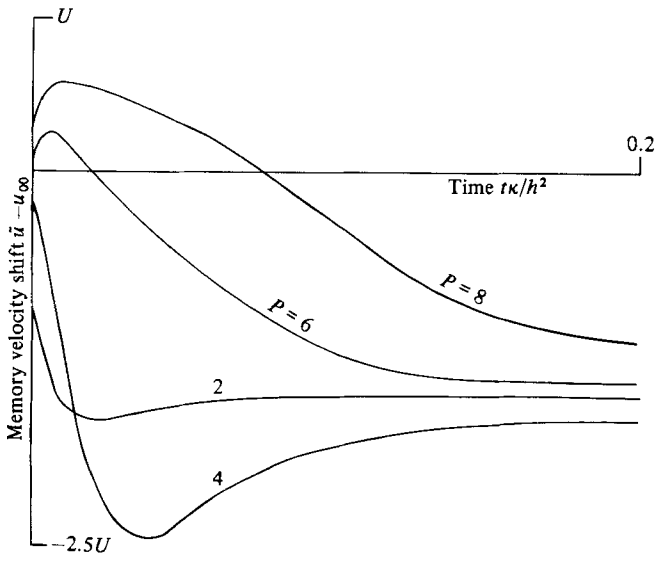

FIGURE 10. The memory displacement velocity $\tilde{u}(\tau)-u_{00}$ for a thermogravitational column, showing the change first to negative and then to positive values as P is increased.

to greatly increased shear dispersion. For example, when $P=0$ we have the respective results

$$\partial_\tau D(0) = \tfrac{128}{105}U^2, \quad D(\infty) = \frac{32}{315}\frac{U^2h^2}{\kappa}, \tag{7.5a}$$

$$\partial_\tau D(0) = \tfrac{1}{5}\bar{u}^2, \quad D(\infty) = \frac{1}{210}\frac{\bar{u}^2h^2}{\kappa}. \tag{7.5b}$$

For large P the equilibrium concentration profile (6.2) is confined to the linear shear region close to the wall. The ratio $8U/3\bar{u}$ of the respective velocity shears gives rise to the ratio $(8U/3\bar{u})^2 = 7.11(U/\bar{u})^2$ between the shear-dispersion rates.

The higher-order velocity coefficients u_{mn} are given by

$$u_{mm} = -\frac{48PU}{m^2\pi^2[m^2\pi^2+P^2]}, \tag{7.6a}$$

$$u_{mn} = \frac{768UPmn}{\pi^2(m^2-n^2)^2[m^2\pi^2+P^2]^{\frac{1}{2}}[n^2\pi^2+P^2]^{\frac{1}{2}}} \quad (m+n \text{ even}), \tag{7.6b}$$

$$u_{mn} = \frac{64Umn(m^2\pi^2+n^2\pi^2+2P^2)}{\pi^2(m^2-n^2)^2[m^2\pi^2+P^2]^{\frac{1}{2}}[n^2\pi^2+P^2]^{\frac{1}{2}}} - \frac{768Unm[\pi^2(m^4+6m^2n^2+n^4)+4P^2(m^2+n^2)]}{\pi^2(m^2-n^2)^4[m^2\pi^2+P^2]^{\frac{1}{2}}[n^2\pi^2+P^2]^{\frac{1}{2}}} \quad (m+n \text{ odd}). \tag{7.6c}$$

Figure 10 shows the time dependence of the memory displacement velocity $\tilde{u}(\tau)-u_{00}$, as given by (4.1). For $P=0$ the up–down symmetry of the flow ensures that $\tilde{u}=u_{00}=0$. As P increases, the smaller amount of contaminant in the downwards-flowing half of the channel gives rise to a trailing tail for the contaminant distribution, and hence to negative values of the skewness and of $\tilde{u}(\tau)-u_{00}$. However, for

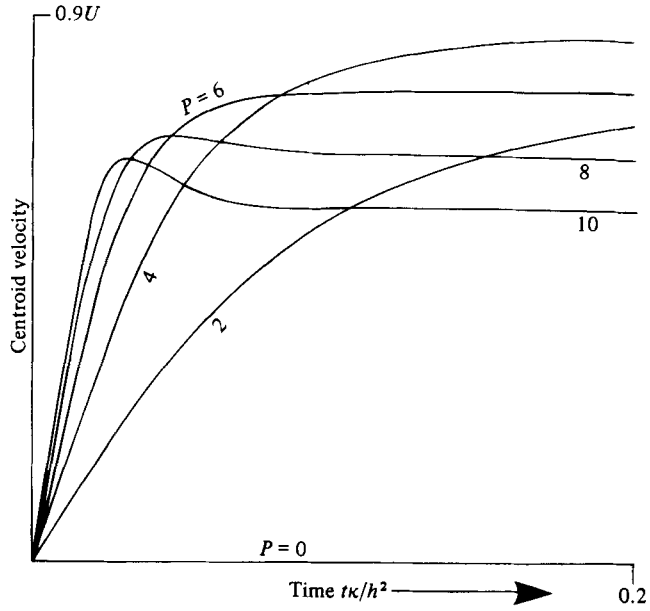

FIGURE 11. The centroid velocity as a function of time for an initially uniform discharge in a thermogravitational column.

sufficiently large P the contaminant is confined so closely to the wall, that the faster-moving fluid slightly further away from the wall gives rise to a forwards tail, positive skewness, and positive values of $\tilde{u}(\tau)-u_{00}$. It is only at large times that the opposing effect of the more distant downwards-going half of the flow tends to counteract this positive skewness, and to make $\tilde{u}(\tau)-u_{00}$ eventually become negative (see (4.2)).

For a uniform discharge the coefficients q_m are the same as for plane Poiseuille flow (6.9). Figure 11 shows the time dependence of the centroid-velocity equation (6.10). As the concentration profile drifts across the flow into the upwards-going fluid, there is an increased centroid velocity. However, for sufficiently large P there is a subsequent decrease in the centroid velocity as the contaminant profile becomes confined to the slow-moving fluid near the wall.

For a mixture of constituents with different transverse Péclet numbers, the crossing-over of the centroid velocity curves implies a delayed separation of the constituents. This feature can be avoided if, as recommended above, the range of Péclet numbers is restricted to the range -3.5 to $+3.5$. With this restriction, it takes a time of order $0.2h^2/\kappa$ for the separation to become fully efficient.

8. Pretreatment

The difference between the centroid velocities for the various species is a maximum for the equilibrium relaxed distribution, and nil for the uniform initial conditions (see figures 5, 11 above). Thus better separation can be achieved if a sample is pretreated by application of the transverse field for a sufficient length of time in a stationary fluid and subsequently eluted. The separation of the constituents is not dependent only upon the centroid velocity. It also depends upon the longitudinal spreading and the skewness of the longitudinal concentration distribution. Hence, to assess the

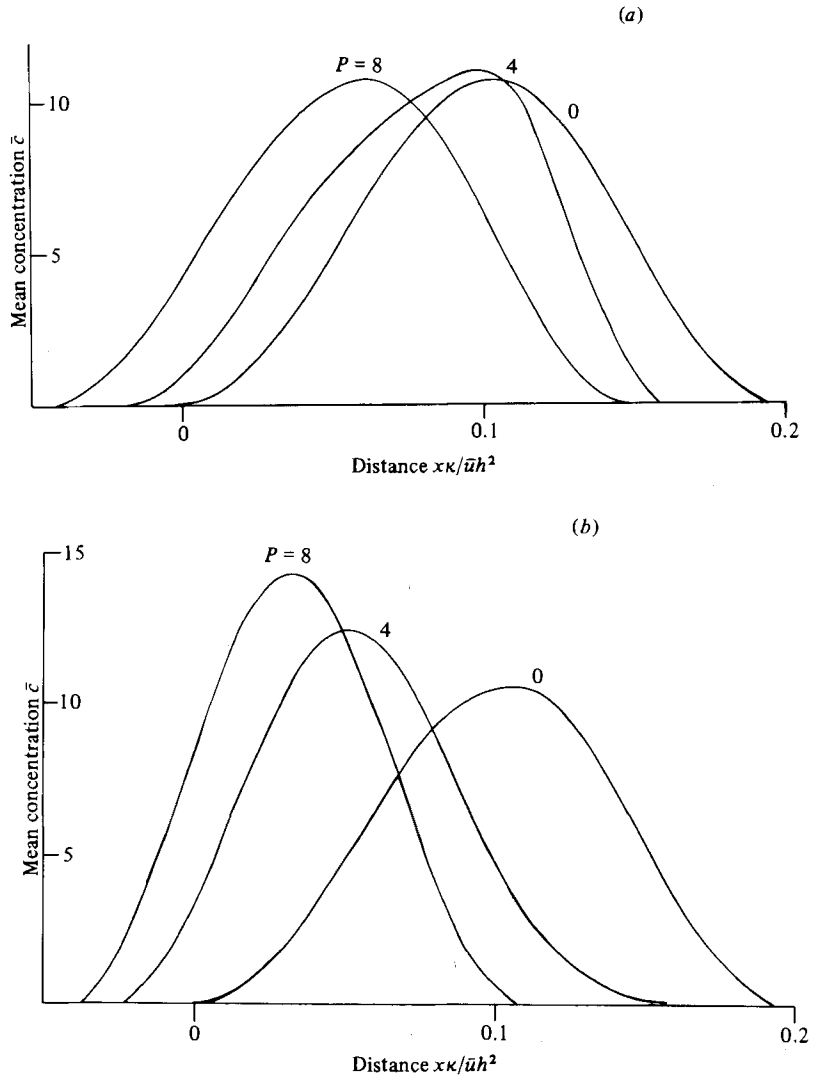

FIGURE 12. Contaminant distributions for (*a*) uniform discharges, and (*b*) pretreated (equilibrium) discharges in plane Poiseuille flow.

worthwhileness of pretreatment it is desirable to compute the concentration distributions for a range of transverse Péclet numbers, with and without pretreatment.

At large times the initial conditions become unimportant. Yet at small times the separation process is dominated by the longitudinal spreading. Thus it is at intermediate times, of order $1/\lambda_1$, that the effects of pretreatment will be most noticeable. This is precisely the time range for which the delay-diffusion equation (5.4) is both accurate and a significant improvement over the variable-coefficient diffusion equation (5.5) (see figure 6). Hence to assess the pretreatment technique we confidently make use of the model equation (5.4).

For plane Poiseuille flow we find that pretreatment is quite effective. Figures 12(*a*, *b*) show the concentration distributions for uniform and for equilibrium discharges at the time $t = 0.1h^2/\kappa$. The improved separation owes as much to the

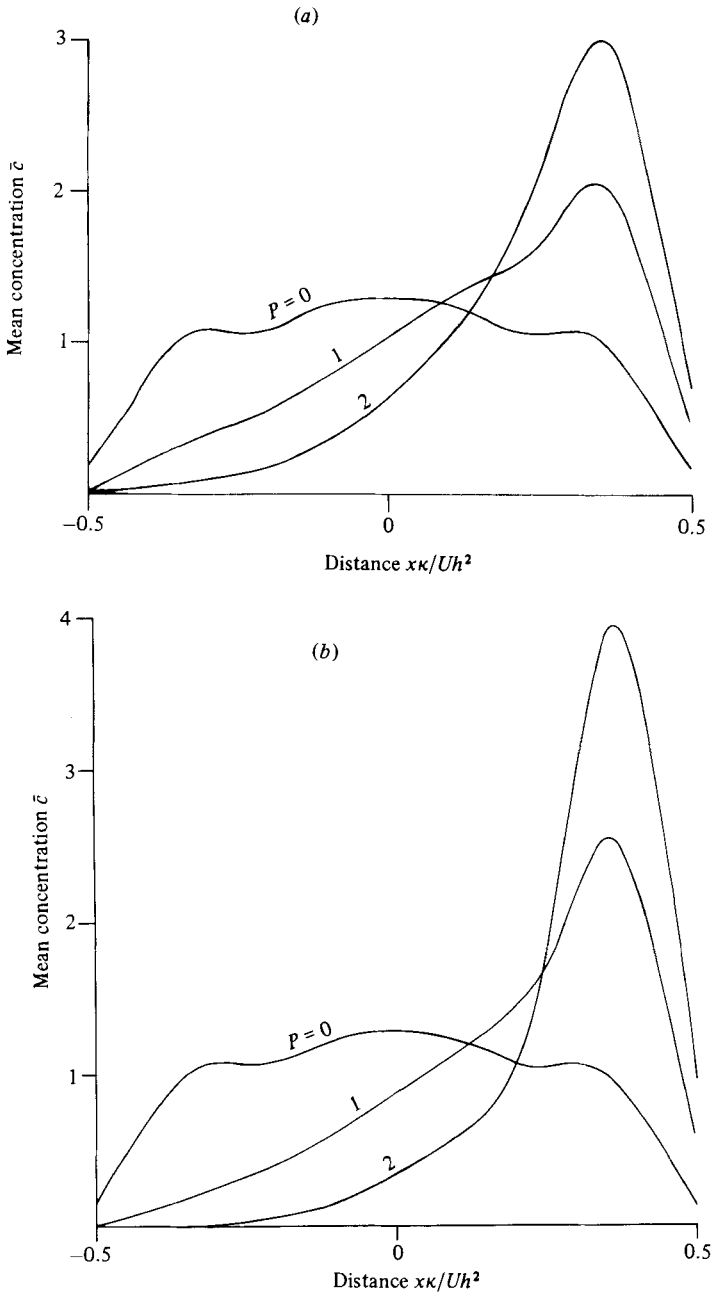

FIGURE 13. Contaminant distributions for (*a*) uniform, and (*b*) pretreated (equilibrium) discharges in a thermogravitational column.

reduced net longitudinal spreading as to the increased centroid displacement. Another contributory factor is that the skewness increases with P and shifts the concentration peaks further to the left.

Alas, for thermogravitational columns the pretreatment technique turns out to be of little use. Figures 13(*a*, *b*) show the concentration distributions for uniform and for equilibrium discharges at the time $t = 0.4h^2/\kappa$. The effect of the increasingly

negative skewness almost exactly annuls the centroid shift, and the position of the concentration peak is almost the same whether $P = 1$, 2 or if there is pretreatment or not. All that is affected is the height of the concentration peak.

From these two examples we infer that, for pretreatment to be useful, the skewness should augment the centroid displacement, thereby making the separation process quite rapid. When these two effects are in opposition the influence of the discharge conditions (uniform or pretreated) will have become insignificant by the time that separation has taken place.

I wish to thank a referee for drawing my attention to the pretreatment technique, and to the implications derivable from the above analysis. The financial support of British Petroleum and the Royal Society is gratefully acknowledged.

REFERENCES

GIDDINGS, J. C. 1968 Nonequilibrium theory of field-flow fractionation. *J. Chem. Phys.* **49**, 81–85.

GRADSHTEYN, I. S. & RHYZHIK, I. M. 1965 *Tables of Integrals, Series and Products.* Academic.

JAYARAJ, K. & SUBRAMANIAN, R. S. 1978 On relaxation phenomena in field-flow fractionation. *Sep. Sci.* **13**, 791–817.

KIRKWOOD, J. G. & BROWN, R. A. 1952 Diffusion–convection. A new method for the fractionation of macromolecules. *J. Am. Chem. Soc.* **74**, 1056–1058.

KRISHNAMURTHY, S. & SUBRAMANIAN, R. S. 1977 Exact analysis of field-flow fractionation. *Sep. Sci.* **12**, 347–379.

LIGHTFOOT, E. N., CHIANG, A. S. & NOBLE, P. T. 1981 Field-flow fractionation (polarisation chromatography). *Ann. Rev. Fluid Mech.* **13**, 351–378.

LURE, M. V. & MARON, V. I. 1979 Solid particle impurity propagation in a fluid flow in a pipe. *J. Engng Phys.* **36**, 562–567.

SMITH, R. 1981 A delay-diffusion description for contaminant dispersion. *J. Fluid Mech.* **105**, 469–486.

SMITH, R. 1982 Non-uniform discharges of contaminants in shear flows. *J. Fluid Mech.* **120**, 71–89.

TAGGART, A. F. 1953 *Handbook of Mineral Dressing.* Wiley.